Amidase and Lysozyme Dual Functions in TseP Reveal a New Family of Chimeric Effectors in the Type VI Secretion System

Running title: Chimeric effector with dual functions

Zeng-Hang Wang[1,2], Ying An[2], Ting Zhao[3,4], Tong-Tong Pei[2], Dora Yuping Wang[2,5], Xiaoye Liang[2], Wenming Qin[3*], Tao Dong [2*]

Affiliations:

[1] State Key Laboratory of Microbial Metabolism, Joint International Research Laboratory of Metabolic & Developmental Sciences, School of Life Sciences and Biotechnology, Shanghai Jiao Tong University, Shanghai, 200240, China

[2] Department of Immunology and Microbiology, School of Life Sciences, Southern University of Science and Technology, 518055, Shenzhen, China

[3] National Facility for Protein Science in Shanghai, Shanghai Advanced Research Institute, Chinese Academy of Sciences, Shanghai, 201210, People's Republic of China

[4] School of Pharmaceutical Sciences, Wuhan University, Wuhan, China

[5] Department of Physiology, University of Toronto, Toronto, Canada

[*] Correspondence to dongt@sustech.edu.cn；qinwenming@sari.ac.cn

Keywords: protein secretion, effector, peptidoglycan, amidase, synthetic biology

Abstract

Peptidoglycan (PG) serves as an essential target for antimicrobial development. An overlooked reservoir of antimicrobials lies in the form of PG-hydrolyzing enzymes naturally produced for polymicrobial competition, particularly those associated with the type VI secretion system (T6SS). Here we report that a T6SS effector TseP, from *Aeromonas dhakensis*, represents a family of effectors with dual amidase-lysozyme activities. *In vitro* PG-digestion coupled with LC-MS analysis revealed the N-domain's amidase activity, which is neutralized by either catalytic mutations or the presence of the immunity protein TsiP. The N-domain, but not the C-domain, of TseP is sufficient to restore T6SS secretion in T6SS-defective mutants, underscoring its critical structural role. Using pull-down and secretion assays, we showed that these two domains interact directly with a carrier protein VgrG2 and can be secreted separately. Homologs in *Aeromonas hydrophila* and *Pseudomonas syringae* exhibited analogous dual functions. Additionally, N- and C-domains display distinctive GC contents, suggesting an evolutionary fusion event. By altering the surface charge through structural-guided design, we engineered the $TseP^{C4+}$ effector that successfully lyses otherwise resistant *Bacillus subtilis* cells, enabling the T6SS to inhibit *B. subtilis* in a contact-independent manner. This research uncovers TseP as a new family of bifunctional chimeric effectors targeting PG, offering a potential strategy to harness these proteins in the fight against antimicrobial resistance.

Significance Statement

Antimicrobial resistance urgently demands global interventions, and the bacteria cell wall remains a promising target. Our research introduces a novel family of bifunctional, cell-wall-damaging T6SS effectors. More importantly, we demonstrate an effective strategy to enable an otherwise ineffective enzyme to target both Gram-negative and Gram-positive bacteria. Our findings highlight a promising path forward using cell-wall-damaging effectors, a largely untapped resource, in the fight against antimicrobial resistance.

Introduction

Antimicrobial resistance (AMR) is a critical global health crisis, with bacterial AMR implicated in approximately 4.95 million deaths in 2019, and predictions estimating up to 10 million deaths per year by 2050 (*1*, *2*). Developing novel antimicrobials is thus of paramount importance but also a highly challenging task. Bacterial cell walls, mainly composed of peptidoglycan (PG) and crucial for survival, serve as a primary target for antimicrobials. However, the discovery of conventional PG-inhibiting small molecules is impeded by fewer choices and increasing resistance (*3*, *4*). The naturally occurring PG-lysing enzymes, secreted by bacteria for competition in polymicrobial environments (*5–8*), remain underexplored for AMR treatment.

As a widespread molecular weapon in Gram-negative bacteria, the type VI secretion system (T6SS) can directly inject PG-lysing enzymes and other antibacterial toxins into neighboring microbes and anti-eukaryotic toxins to yeast and mammalian cells(*7*, *9–15*). The conserved structure of T6SS consists of a double tubular structure, a baseplate TssEFGK complex, and a transmembrane TssJLM complex (*16–19*). A spear-like inner tube, made of stacks of Hcp hexamers, is ejected outward upon contraction of an outer sheath made of stacks of TssB/C hexamers, and a VgrG-PAAR spike complex sitting atop the Hcp tube is delivered concomitantly (*12*, *20*, *21*). Although the ejected Hcp spear can penetrate neighboring bacterial cells, T6SS-elicited damages are largely dependent on the secreted effectors rather than the penetration (*22–24*). Numerous T6SS effectors have been predicted in Gram-negative bacteria, and known effectors display diverse functions including damaging the cell wall and membrane, DNase, metal scavenging, and targeting host cell actin cytoskeleton (*6*, *25–32*). Despite the functional diversity of T6SS effectors, PG-targeting effectors seem to be most commonly associated with the T6SSs.

The conserved structure of PG comprises repeating disaccharide units of N-acetylglucosamine (NAG) and N-acetylmuramic acid (NAM), with a short peptide (most commonly $_{L}$-Ala-$_{D}$-Glu-*m*-DAP-$_{D}$-Ala-$_{D}$-Ala) attached to each NAM (*33*). Adjacent peptide chains of PG are cross-linked, forming a

51 continuous network that envelops bacterial cells (*33*). T6SS effectors known to target PG fall into two
52 categories, T6SS amidase/endopeptidase (Tae) families cleaving the peptides and T6SS glycoside
53 hydrolase (Tge) families cleaving the glycan backbone. Tae effectors have been found to cleave bonds
54 between D-Glu and *m*DAP, between *m*DAP and D-Ala, and between NAM and L-Ala (*7*, *27*, *34*, *35*). Tge
55 effectors possess β-(1-4)-N-acetyl-muramidase activities and N-acetylglucosaminidase activities (*5*, *6*,
56 *27*, *36*). The recent discovery of Tse4 in *Acinetobacter baumannii*, cleaving both the glycan strand and
57 the crosslinked peptide cross-bridge, suggests dual enzymatic activities could be found in a single
58 effector (*10*). However, such bifunctionality among effectors is rare.

59 As a ubiquitous waterborne pathogen, *Aeromonas dhakensis* can cause soft tissue infection and
60 bacteremia in fish and humans (*37*, *38*). The T6SS of *A. dhakensis* type strain SSU is active under
61 laboratory conditions and can secrete three known antimicrobial effectors, a membrane-targeting TseC,
62 a lysozyme-like TseP, and a nuclease TseI (*25*, *39–42*). Our previous findings have established that TseP
63 serves a structural role because its expression can restore the T6SS secretion in the Δ*3eff* mutant lacking
64 all three effector genes, and the C-terminal domain, $TseP^C$, possesses lysozyme activities (*40*). However,
65 the function of the N-terminal domain, $TseP^N$, which lacks any recognizable conserved motif, has
66 remained elusive. This study unveils $TseP^N$ is capable of cleaving the peptide link between NAM and L-
67 Ala as an amidase. Both $TseP^N$ and $TseP^C$ can be secreted separately by the T6SS, but only $TseP^N$ can
68 compensate for T6SS defects, indicating its critical role as a structural component. Additionally, $TseP^N$
69 exhibits approximately 10% higher GC content than $TseP^C$, and homologs of $TseP^N$ and $TseP^C$ exist
70 independently in divergent species. This disparity in GC content and the presence of domain-specific
71 homologs suggest an evolutionary fusion event. We further show that $TseP^C$ can be engineered to
72 hydrolyze resistant Gram-positive *Bacillus subtilis* cells, conferring the T6SS with the capability to kill
73 Gram-positive bacteria in a contact-independent manner. This research identifies a novel class of
74 amidase-lysozyme bifunctional effectors, provides insights into effector evolution, and highlights the
75 potential of engineering these effectors as antimicrobials.

76

77 **Results**

78 **TseP^N and TseP^C can be independently secreted by the T6SS**

79 To delineate the regions of TseP crucial for T6SS-mediated secretion, we constructed two TseP
80 truncations, TseP^N and TseP^C, and then expressed them in the Δ*3eff* mutant using the pBAD arabinose-
81 inducible vectors. Consistent with our previous results (*40*), protein secretion assays show that the Δ*3eff*
82 mutant, akin to the T6SS null Δ*vasK*, failed to secrete Hcp (Figure 1A, Supplemental Figure S1).
83 Complementation with TseP and TseP^N, but not TseP^C, restored Hcp secretion, despite at a reduced level
84 relative to the wild type (Figure 1A). We next tested whether the T6SS assembly is restored using a
85 chromosomal sheath-labeled construct TssB-sfGFP (*40*). Fluorescence microscopy analysis showed that
86 complementation with both TseP and TseP^N, but not the TseP^C, restored sheath assembly (Figure 1, B
87 and C). Because both Hcp secretion and sheath assembly are hallmarks of T6SS assembly, these findings
88 highlight the important structural role of the TseP N-terminus.

89 Interestingly, we noticed that TseP^N, but not TseP^C, was secreted (Figure 1A). The lack of TseP^C
90 secretion might be due to a defective T6SS. To test this, we expressed different plasmid-borne TseP
91 constructs in a panel of SSU mutant strains. Western blot analysis not only confirmed the secretion of
92 TseP and TseP^N but also detected the secretion of TseP^C, albeit to a lesser extent, in both wild-type and
93 the Δ*tseP* cells (Figure 1D). Considering that VgrG2 is the carrier protein for TseP delivery (*40*), we next
94 tested whether TseP^N and TseP^C could interact with VgrG2. Pull-down analysis showed direct interaction
95 of VgrG2 with TseP^N and TseP^C, in contrast to the sfGFP and MBP negative controls (Figure 1E). These
96 results indicate TseP^N and TseP^C can be secreted independently by the T6SS.

97 **TseP^N is a Zn^{2+}-dependent amidase**

98 When analyzing TseP-mediated PG hydrolysis products using ultraperformance liquid
99 chromatography coupled with mass spectrometry (UPLC-MS), we detected two distinctive peaks and
100 determined their corresponding products to be NAM-NAG disaccharides and Tri/Tetra peptides (Figure

101 2, A and B), the latter suggesting an amidase activity. The released peptides were also detected in samples
102 treated with $TseP^{N}$ and the catalytically inactive C-terminal lysozyme mutant $TseP^{E663A}$ (*40*), but not
103 with $TseP^{C}$ or its inactive $TseP^{C\text{-}E663A}$ mutant, indicating that the amidase activity is attributed to $TseP^{N}$.
104 Sequence comparison with known amidases suggests that the $TseP^{N}$ contains a predicted Zn^{2+}
105 binding domain with several conserved residues H19, H23, H109, H339, H359, and E539 (Figure 2C).
106 To test the effect of these residues on the $TseP^{N}$ amidase, we replaced these sites with alanine using site-
107 directed mutagenesis and then purified a set of $TseP^{N}$ mutant proteins. Subsequent PG-digestion assays,
108 coupled with UPLC-MS analysis, showed significantly reduced amidase activity in these mutants
109 compared to $TseP^{N}$ (Figure 2D).
110 To test the role of metal ions for TseP's amidase activity, we added the chelating agent EDTA to
111 the PG-digestion mixture, which abolished the amidase activity (Figure 2E). To further identify the
112 specific metal ion involved, we also purified TseP in the presence of EDTA and then supplemented it
113 with Zn^{2+}, Ca^{2+} and a combination of both. PG-digestion assays revealed that adding Zn^{2+}, but not Ca^{2+},
114 restored the amidase function (Figure 2E).
115 Given the dual functionality of TseP, we sought to determine if TsiP, known as the immunity
116 protein neutralizing the lysozyme activity, could inhibit the amidase, by mixing purified TsiP with TseP,
117 $TseP^{N}$, and $TseP^{C}$ in varying molar ratios. Enzymatic assays using purified PG showed that TsiP could
118 effectively inhibit both amidase activity and peptidoglycan hydrolysis activity of TseP, $TseP^{N}$ and $TseP^{C}$
119 (Figure 2F, Supplemental Figure S2). Additionally, pull-down assays showed that TsiP interacts with not
120 only $TseP^{C}$ but also $TseP^{N}$ (Figure 2G). Collectively, these results indicate that $TseP^{N}$ is a Zn^{2+}-dependent
121 amidase.

122 **Amidase activity is not required for T6SS assembly or lysozyme function**

123 To determine whether the amidase activity is important for the structural role of $TseP^{N}$, we
124 expressed these amidase-inactive mutants in the Δ*3eff* TssB-sfGFP mutant and tested T6SS-related
125 functions. Secretion analysis revealed that expression of $TseP^{H339A}$, but not the other mutants, restored

126 Hcp secretion similar to wild-type TseP (Figure 3A). As control, we examined the expression of these
127 TseP variants and found comparable signals in the cell lysates and secretion samples. Observations of
128 TssB-sfGFP sheath assembly in the Δ*3eff* TssB-sfGFP mutant further supported these findings, with the
129 $TseP^{H339A}$ strain showing dynamic assembly of T6SS similar to the strain expressing the wild-type
130 protein (Figure 3B, Supplemental Figure S3, A and C). Further analysis through bacterial competition
131 assays, with *E. coli* MG1655 strain as prey, mirrored these results (Figure 3C). The expression of
132 $TseP^{H339A}$ and TseP showed comparable killing abilities while the expression of other mutants
133 demonstrated severely impaired killing activities as the T6SS defective Δ*3eff* (Figure 3C). Although it is
134 unclear why the other mutations failed to complement, the H339A amidase-inactive mutation exhibiting
135 a similar complementary role to wild type TseP suggests that the amidase activity is not required for
136 T6SS assembly.

137 Additionally, we tested whether there is any synergistic effect between amidase and the $TseP^{C}$-
138 mediated lysozyme activities by comparing PG degradation treated with TseP, $TseP^{C}$, and $TseP^{H339A}$.
139 Results showed that TseP exhibited higher glycoside hydrolase activities than the $TseP^{C}$ alone, but there
140 was no difference between TseP and the $TseP^{H339A}$ mutant (Figure 3D, Supplemental Figure S3B). This
141 indicates that amidase and lysozyme activities can each operate as functional modules within the protein.

142 **TseP homologs exhibit similar dual functions**

143 Homolog searching analysis reveals a broad distribution of TseP homologs across Gram-negative
144 bacteria (Figure 4A, Supplemental Figure S4). To examine the dual functionality of these homologs, we
145 selected two representative proteins that have not been previously characterized: AHA_1849 from
146 *Aeromonas hydrophila* which is a closely related homolog from the same genus, and PSPTO_5204 from
147 *Pseudomonas syringae*, a more distantly related homolog. To determine whether AHA_1849 and
148 PSPTO_5204 share amidase and lysozyme activities as TseP, we expressed and purified their respective
149 N- and C-terminal truncated mutants, AHA_1849^{N} (1-640aa), AHA_1849^{C} (641-851aa), $PSPTO_5204^{N}$
150 (1-343aa), and $PSPTO_5204^{C}$ (344-588aa) (Supplemental Figure S4). We also constructed inactivating

151 mutations in their predicted catalytic residues for each protein to serve as controls (Supplemental Figure
152 S4). Subsequent PG-hydrolysis and UPLC-MS analysis confirmed that both AHA_1849 and
153 PSPTO_5204 exhibit dual amidase and lysozyme activities, capable of cleaving both peptide and glycan
154 chains (Figure 4, B and C).

155 Additionally, by analyzing the GC-contents of the two *Aeromonas* homologs, we found that the
156 GC-content of $TseP^N$ is about 10% higher than that of $TseP^C$ and 10% lower than the upstream VgrG
157 (Figure 4D). This suggests that these two domains might have been horizontally transferred and
158 subsequently fused during evolution. To explore this hypothesis further, we searched for homolog
159 proteins with similar structures to either $TseP^N$ or $TseP^C$ in the Foldseek Search AFDB50 database (*43*),
160 yielding 1000 proteins with comparable predicted structures. We identified $TseP^N$-only homologs in
161 various *Aeromonas* species, including a specific homolog in *A. schubertii* possessing only the $TseP^N$
162 domain, whereas $TseP^C$-homologs were discovered in several other species, such as *Fulvimonas soli* and
163 *Vibrio campbellii* (Figure 4E). The comparison of their predicted structures reveals high similarity
164 (Figure 4F, Supplemental Table S2 and S3). Considering the GC-content difference, we postulate that
165 $TseP^N$ and $TseP^C$ domains may have been fused through a recombination event, resulting in a chimeric,
166 dual-functional TseP.

167 **Crystallographic analysis of $TseP^C$ reveals a wide active groove**

168 While testing TseP-mediated hydrolysis of purified PG from Gram-negative bacteria, we noticed
169 that both TseP and $TseP^C$ displayed more efficient digestion than the commonly used hen-egg lysozyme
170 (Figure 5A). This enhanced activity suggests that TseP may utilize a unique mechanism for cell wall
171 degradation. To further investigate this, we determined the X-ray crystal structure of $TseP^C$ to a resolution
172 of 2.27Å (R_{work} =0.189 and R_{free}=0.227), by molecular replacement with one molecule in the asymmetric
173 unit (Table 1).

174 The crystal structure revealed that $TseP^C$ comprises a smaller lobe of seven helices and a larger
175 lobe of ten helices, separated by a concave groove (Figures 5B, Supplemental Figure S5A). The surface

176 electrostatic potential of $TseP^{C}$, calculated using the Adaptive Poisson-Boltzmann Solver (APBS),
177 consists of both electronegative and electropositive regions, unlike the predominantly electronegative
178 groove of lysozyme (Figure 5C, Supplemental Figure S5B). The electropositive surface of $TseP^{C}$ consists
179 of residues R723 and K796, with an adjacent residue Y720 corresponding to W62 in lysozyme, altering
180 which is known to affect substrate binding (*44*). Additionally, the previously predicted catalytic dyad
181 (E655 and E663) was located near the groove. Although this structural arrangement resembles that of
182 other lysozyme family members, $TseP^{C}$ exhibits a less compact conformation with a notably wider
183 groove compared to the typical lysozyme (Figure 5D). Previous studies have shown that the lysozyme
184 possesses catalytic sites at E53 and D70 in the substrate-binding groove (*44*), while the active residues
185 in the $TseP^{C}$ structure are E654 and E663, respectively (Figure 5D). To test the effect of E663 for $TseP^{C}$
186 activity, we purified a mutant E663D ($TseP^{C\text{-}E663D}$) protein and perform PG digestion assays. The results
187 show that $TseP^{C\text{-}E663D}$ lost the activity, suggesting the greater distance within the groove requires this
188 glutamate residue (Figure 5E). These results collectively highlight the key structural features that may
189 account for the increased activity of $TseP^{C}$ relative to the hen-egg lysozyme.

190 **Engineered $TseP^{C}$ can lyse Gram-positive cells**

191 To test whether TseP can degrade various cell walls, we purified PG from *B. subtilis*, a model
192 Gram-positive bacterium, for use as substrate. However, we failed to detect any PG hydrolysis treated
193 with TseP or $TseP^{C}$, in contrast to the lysozyme (Figure 6A). Further purification of PG with NaOH
194 treatment, removing PG-associated peptides, led to effective hydrolysis of PG by TseP and $TseP^{C}$,
195 suggesting a difference in substrate accessibility between the lysozyme and TseP. By comparing protein
196 surface electrostatic potentials between the lysozyme and $TseP^{C}$, we noticed a more electronegative
197 surface patch in $TseP^{C}$, suggesting a potential electrostatic repulsion from negatively charged PG (Figure
198 6B, Supplemental Figure S5B). To increase electropositive regions while minimizing impact on activity,
199 we mutated four negative charge residues distant from the active site and obtained a quadruple mutant
200 $TseP^{C4+}$ (Figure 6B). Activity assays confirmed that $TseP^{C4+}$ retained *E. coli* PG-hydrolyzing activities

201 (Figure 6C). To test whether the engineered TseP^{C4+} was able to lyse *B. subtilis*, we treated *B. subtilis*
202 cells with purified TseP^{C} and TseP^{C4+} and found that cells were lysed effectively by TseP^{C4+} but not
203 TseP^{C} (Figure 6D, Supplemental Figure S5C). These results indicate that modulating the surface charge
204 is an effective strategy to expand the target range of PG-lysing effectors.

205 Next, we tested whether the engineered TseP^{C4+} could be delivered by the T6SS for inhibiting *B.*
206 *subtilis*. Protein secretion analysis showed a significant TseP^{C4+} signal in secretion samples, despite at a
207 lower level than the wild type TseP^{C} (Figure 6E). When *B. subtilis* was co-incubated with the Δ*tseP*
208 mutant expressing the engineered TseP^{C4+} in liquid culture, survival of *B. subtilis* was significantly
209 reduced in a T6SS-dependent manner (Figure 6F, Supplemental Figure S5D). These data collectively
210 suggest that the T6SS can be armed with engineered TseP^{C4+} to gain Gram-positive killing capabilities
211 in a contact-independent manner.

212

213 **Discussion**

214 The T6SS plays a pivotal role in bacterial competition, using a variety of antibacterial effectors
215 to kill competing cells. The exploration of effector functions holds the promise of unlocking a largely
216 untapped source of novel antimicrobials, presenting innovative approaches to address the escalating
217 antimicrobial resistance crisis. Here we report that TseP represents a novel family of dual-functional
218 chimeric effectors, exhibiting both amidase and lysozyme activities. Our study reveals that the N-
219 terminus of TseP not only serves a critical structural role in T6SS assembly but also acts as a Zn^{2+}-
220 dependent amidase. The N- and C-domains are both secreted and functionally independent, and may be
221 subject to an evolutionary fusion event to form the chimeric full-length TseP. Such multifunctionality
222 underscores a complex evolutionary strategy aimed at promoting T6SS-mediated competitiveness.

223 Among the known T6SS effectors, those targeting the bacterial PG layer represent a prevalent
224 category. Certain T6SSs are capable of translocating multiple PG-targeting effectors. For instance, the
225 H1-T6SS in *Pseudomonas aeruginosa* deploys Tse1 and Tse3, while *Vibrio cholerae* secretes VgrG3

226 and TseH (*5–7*, *9*, *45*, *46*). Tse1 and TseH exhibit endopeptidase activities, whereas Tse3 and VgrG3
227 have potent lysozyme activities (*5–7*, *9*, *45*, *46*). Yet, it remains relatively uncommon to identify effectors
228 that possess dual functionality, capable of cleaving both the glycan chains and the cross-linked peptides
229 within the bacterial cell wall. To date, the sole established example is Tse4 from *A. baumannii*, which
230 acts both as a transglycosylase to cleave the glycan strand and as an endopeptidase to cut the peptide
231 cross-bridge (*10*, *47*, *48*). Our enzymatic assays reveal that TseP distinguishes itself from Tse4 with dual
232 roles as a lysozyme and an amidase, as well as a structural role for T6SS assembly. Further homology
233 searches and biochemical validations of homolog activities substantiate that TseP constitutes a new
234 family of dual-functional effectors.

235 Our data demonstrate that the N-terminus of TseP can modulate T6SS assembly, which provides
236 further evidence that effectors play a crucial structural role in T6SS assembly (*23*, *39*, *49*, *50*). Although
237 this notion has now been shown in several species, the molecular details remain elusive. The assembly
238 of a non-contractile mutant T6SS in *V. cholerae* in the absence of effectors suggests that effectors might
239 be needed to stabilize a polymerizing T6SS (*51*). In comparison to $TseP^{C}$, the N-terminus not only
240 contributes to T6SS assembly but also exhibits 10% higher GC content. Additionally, both N and C-
241 terminus can be independently secreted by the T6SS. Using structure-assisted homolog search, we have
242 identified $TseP^{N}$ and $TseP^{C}$-only proteins in different species. These data suggest that these two domains
243 may result from independent effector proteins and have undergone an evolutionary fusion event.

244 Previous studies have shown that expressing TseP in the periplasm is highly toxic, but this
245 toxicity is mitigated when catalytic mutations are introduced into the C-terminal lysozyme domain (*40*).
246 This indicates that the N-terminal amidase is either less toxic or is tightly regulated by the concentration
247 of Zn^{2+} in the growth medium. Although the total intracellular Zn^{2+} concentration during growth in LB
248 has been reported to be around 0.1mM—approximately 100 times higher than the Zn^{2+} level in the LB
249 medium—the bioavailable (free) Zn^{2+} concentration within *E. coli* cells remains exceedingly low (*52*).
250 A similar dependency on metal ions was observed with another cell-wall-targeting endopeptidase

251 effector, TseH, whose activity is dependent on the environmental concentrations of Mg^{2+} and Ca^{2+} (*53*).
252 Such metal ion dependencies might lead to misbelief about these effectors being cryptic or inactive,
253 complicating the discovery and functional analysis of these important proteins.

254 TseP is predicted to contain an EF-hand calcium-binding domain with a "helix-loop-helix" motif,
255 a feature previously unreported in T6SS effectors (Supplemental Figure S6A). However, mutations
256 introduced to this domain, aimed at exploring its role in T6SS assembly and TseP toxicity, did not reveal
257 any critical effect on TseP functions under the conditions tested (Supplemental Figure S6, B and C). It is
258 possible that this EF-hand motif is active under more Ca^{2+} stringent conditions or during infections.
259 Further study is required to decipher its physiological function. Additionally, while constructing TseP
260 variants with different residue changes, we noticed that even single residue changes could reduce the
261 expression, secretion or the structural role of TseP, highlighting the technical challenge of heterologous
262 effector engineering (Figure 3A, Supplemental Figure S7, A and B).

263 Because the outer membrane of Gram-negative bacteria generally prohibits the entry of cell-wall
264 lysing proteins, the relatively exposed Gram-positive bacteria are likely more amenable to such
265 treatments. However, the T6SS, exclusively found in Gram-negative bacteria, primarily targets Gram-
266 negative species. To date, only two T6SSs, identified in *Acidovorax citrulli* and *A. baumannii* (*10*, *13*),
267 have shown the capability to kill Gram-positive bacteria. Additionally, no Gram-positive cell wall lysing
268 effectors have been reported; for instance, Tse4 from *A. baumannii* cannot directly lyse *B. subtilis*
269 cultures but requires T6SS delivery. Our biochemical characterization and engineering of $TseP^{C}$ not only
270 establishes its exceptional enzymatic activity but also demonstrates an effective strategy to acquire Gram-
271 positive-cell lysing activities, as well as to equip the T6SS of *A. dhakensis* with a contact-independent
272 killing ability. These results highlight the potential of antimicrobial effector engineering in addressing
273 antimicrobial resistance.

274 In conclusion, our study unveils a new family of dual functional chimeric T6SS effectors and
275 demonstrates the potential for bioengineering these proteins to broaden their antimicrobial spectrum. The

276 engineered $TseP^C$ represents the first effector variant capable of directly lysing *B. subtilis* cultures, paying
277 the way for engineering the diverse set of T6SS cell-wall targeting effectors. The urgent need for new
278 antimicrobials necessitates the exploration of innovative strategies. The insights from our research into
279 T6SS and its diverse effectors signal promising directions for future work in microbial biology and
280 antimicrobial therapy. When enhanced through protein engineering, these enzymes have the potential to
281 address bacterial infections not only in medical settings but also in food safety and animal health.

282 **Materials and Methods**

283 **Bacterial strains and growth conditions**

284 All strains and plasmids used in this study are displayed in Supplemental Table S1. Strains were routinely
285 cultivated in Lysogeny Broth (LB) ([w/v] 1% tryptone, 0.5% yeast extract, 0.5% NaCl) under aerobic
286 conditions at 37 °C. Antibiotics were supplemented at the following concentrations: streptomycin (100
287 μg/ml), kanamycin (50 μg/ml), gentamicin (20 μg/ml), chloramphenicol (25 μg/ml for *E. coli*, 2.5 μg/ml
288 for SSU). All plasmids were constructed using standard molecular techniques, and their sequences were
289 verified through Sanger sequencing. All strains and plasmids are available upon request.

290 **Protein secretion assay**

291 Secretion assays were performed as previously described (*40*). Briefly, cells were grown in LB to
292 OD_{600}=1 and collected by centrifugation at 2,500 × *g*. The pellets were resuspended in fresh LB and
293 incubated at 28 °C for 2 h with 0.01% (w/v) L-arabinose. After incubation, cells were pelleted again by
294 centrifugation at 2,500 × *g* for 8 min. Cell pellets were then resuspended in SDS-loading dye and used
295 as cell lysate samples. The supernatants were centrifuged again at 12,000 × *g* for 30 s and then
296 precipitated in 10% (v/v) TCA (trichloroacetic acid) at -20 °C for 30 min. Precipitated proteins were
297 collected by centrifugation at 15,000 × *g* for 30 min at 4 °C, and then washed twice with acetone. The
298 air-dried pellets were resuspended in SDS-loading dye and used as the secreted protein samples. All the
299 samples were boiled for 10 min before SDS-PAGE analysis.

300 **Western blotting analysis**

301 Proteins were separated using SDS-PAGE and subsequently transferred onto a PVDF membrane (Bio-
302 Rad). Prior to antibody incubation, the membrane was blocked with a solution of 5% (w/v) non-fat milk
303 dissolved in TBST buffer (consisting of 50 mM Tris, 150 mM NaCl, 0.1% [v/v] Tween-20, pH 7.6) for
304 1 h at room temperature. The membrane was then incubated sequentially with primary and secondary
305 antibodies. The Clarity ECL solution (Bio-Rad) was utilized for signal detection. Monoclonal antibodies
306 specific to RpoB (RNA polymerase beta subunit) were sourced from Biolegend (Product # 663905).
307 Additionally, polyclonal antibodies to Hcp were customized by Shanghai Youlong Biotech (*41*). HRP-
308 linked secondary antibodies were purchased from Beyotime Biotechnology (Product # A0208 and #
309 A0216, respectively).

310 **Protein expression and purification**

311 Proteins were expressed using pET28a vector with the His tag in *E. coli* BL21 (DE3). Strains containing
312 the recombinant plasmid were grown in LB at 37 °C. When the optical density of the culture reached
313 OD_{600} of 0.6, isopropyl-β-D-thiogalactopyranoside (IPTG) was added to a final concentration of 1 mM,
314 and the culture was incubated at 20 °C for 16 h. The cells were collected by centrifugation at 2,500 × *g*
315 for 10 minutes at 4°C, resuspended in lysis buffer (20 mM Tris-HCl, 300 mM NaCl, 10 mM imidazole,
316 pH 8.0), and lysed by sonication. After sonication, the lysate was centrifuged at 12,000 × *g* for 60 min at
317 4 °C, and the supernatant was collected. Ni-NTA affinity chromatography was used to purify the target
318 protein, followed by gel filtration using Superdex 200 pg 10/300 column (GE Healthcare). The protein
319 was finally concentrated to 15 mg/ml. All samples were visualized by SDS-PAGE and stained with
320 Coomassie brilliant blue dye. Gel images for all purified proteins used in this study are shown in
321 Supplemental Figure S8.

322 **Crystallization, X-ray data collection and structure determination**

323 $TseP^C$ was crystallized at 18 °C using the hanging drop method. Equal volumes (1:1) of the protein
324 solution and reservoir solution, containing 0.1 M sodium formate (pH 7.0) and 12% (w/v) PEG 3350,

325 were mixed. The crystals were cryoprotected in a mother liquor containing 20% v/v glycol and were
326 flash-cooled at 100 K.
327 An X-ray diffraction data set of $TseP^C$ was collected at beamline BL19U1 (wavelength, 0.97852 Å) at
328 the Shanghai Synchrotron Radiation Facility. Diffraction data was auto-processed by an aquarium
329 pipeline. The crystals were diffracted to 2.27 Å and belonged to the space group C 2 2 21 with unit cell
330 dimensions of a = 44.48 Å, b = 138.8 Å and c = 95.83 Å. This structure was solved by molecular
331 replacement with PHASER using the previously reported SPN1S endolysin structure (PDB ID: 4OK7)
332 as the searching model and further polished by COOT and PHENIX. refine (*54*, *55*). All structure figures
333 were generated using PyMOL (https://pymol.org/2/) software (*56*).

334 **Peptidoglycan purification**

335 Peptidoglycan was extracted as previously described (*57*). Bacteria were cultured at 37 °C for 8 h. Cells
336 were then centrifuged at 4 °C for 30 min at 3,000 × *g* and the cell pellets were washed with ultrapure
337 water. After washing, the bacteria were resuspended in ultrapure water to an OD_{600} of 70-100 and then
338 added dropwise to an equal volume of boiling 8% SDS solution. The mixture was slowly stirred while
339 boiling for 3 h and then cooled naturally to room temperature. The precipitate was collected at 20 °C for
340 1 h at 100,000 × *g* and washed with ultrapure water five times. To remove the residual proteins and DNA,
341 the precipitate was resuspended in 10 ml of 10 mM Tris-HCl (pH 7.0) and treated with 5 mg DNase I
342 and 16 mg trypsin at 37 °C for 16 h. After treatment, the mixture was centrifuged at room temperature
343 for 1 h at 100,000 × *g*, and the pellets were dissolved and treated with an equal volume of boiling 8%
344 SDS solution for another 3 h. The purified peptidoglycan was obtained after washing with ultrapure water,
345 freeze-dried, and stored at -20℃.

346 ***In vitro* enzymatic assays and enzyme kinetics**

347 To characterize the *in vitro* enzymatic activity of TseP and its homologs, 500 μg of purified *E. coli* PG
348 was co-incubated with an equal amount of proteins in a 0.1 ml reaction system at 37 °C for 12 h. After
349 centrifugation, the supernatant was collected and subjected to analysis by ultraperformance liquid

350 chromatography-quadrupole time of flight mass spectrometry (UPLC-QTOF-MS). The Acquity UPLC
351 HSS T3 column was chosen as the solid phase, with solvent A (water with 0.1% [v/v] formic acid) and
352 solvent B (methanol) as the mobile phase. Analyte separation was achieved by a linear gradient of solvent
353 B, which was gradually increased from 1% to 20% over 65 min. Thereafter, a rapid gradient adjustment
354 was followed to increase the concentration of solvent B from 20% to 100% in 1 min, with a retention
355 period of 5 min to ensure complete separation. Finally, the system was flushed with 99% solvent A for
356 4 min to complete the process.
357 To measure the enzyme kinetics of $TseP^C$, a dye-release method was used to detect the PG hydrolyzing.
358 Prior to use, the purified PG was labelled by Remazol Brilliant Blue (RBB) following a previously
359 described method (*58*). Briefly, purified PG was incubated with 20 mM RBB in 0.25 M NaOH for 12 h
360 at 37°C. The RBB-labelled PG was collected via centrifugation for 10 min at 21,400 × *g* and washed
361 with ultrapure water several times until no RBB dye could be detected in the supernatant. This RBB-
362 labelled PG was then applied for the enzyme kinetics analysis. In each reaction, 10 nM enzyme was
363 mixed with different concentrations of RBB-labelled PG at 37°C for 10 min. Undigested PG was pelleted
364 by centrifugation at 21,400 × *g* for 10 min and the dye release in the supernatant was quantified by
365 measuring its absorbance at OD_{595}.
366 **Bacterial competition assays**
367 Killer and prey strains were grown aerobically in liquid LB medium until they reached OD_{600} values of
368 1 and 2, respectively. Later, the cells were harvested via centrifugation and gently resuspended in fresh
369 LB broth. Killer and prey cells mixed at a ratio of 5:1 were deposited onto LB-agar plates supplemented
370 with 0.01% (w/v) L-arabinose and co-incubated for 6 h at 28°C. Afterward, the mixed cells were
371 recovered in fresh LB broth and vigorously vortexed to dislodge the agar. For the Gram-positive bacterial
372 killing, the SSU and *B. subtilis* cells were mixed at a ratio of 20:1 with 0.01% L-arabinose in liquid LB
373 medium for 24 h at 28°C. The mixtures were then serially diluted and plated onto specific antibiotic-
374 containing plates.

375 **Fluorescence microscopic imaging analysis**

376 Bacteria grown to an OD_{600} of 1.0 at 37°C were resuspended in fresh LB medium to achieve a final OD_{600}
377 of 10.0. A 1-μL aliquot was then spotted onto an agarose gel layer containing 0.01% L-arabinose, placed
378 on a clean, dust-free slide, and observed under a microscope (Nikon, Ti2-E). The microscope settings
379 were configured with a 100 × oil objective lens, and GFP signals were visualized using ET-GFP (Chroma
380 49002) parameters. T6SS assembly in bacteria was counted through sequential time-lapse photography
381 over a period of 5 min, with an interval of 10 s between frames. At least three imaging fields were selected,
382 and the number of cells and T6SS assemblies within a representative 30- × 30- μm area in each field
383 were counted.

384 **Bioinformatics analysis**

385 The gene sequences of *A. dhakensis* SSU were retrieved from the draft genome assembly (GenBank
386 accession NZ_JH815591.1) and confirmed by Sanger sequencing. The protein sequence of TseP was
387 analyzed using blastp to identify homologs (*59*). A representative set of the top 14 hits was downloaded
388 from the UniProt (*60*). Phylogeny was constructed using the IQ-tree web server with bootstrap 1000
389 times (*61*). The resulting sequences were then aligned using Clustal Omega (*62*), and the alignment was
390 visualized using ESPript with its default settings (https://espript.ibcp.fr) (*63*).

391 **Data availability**

392 The data that support the findings of this study are available within the article or from the corresponding
393 author upon reasonable request.

394 **Protein Data Bank and accession code**

395 The atomic coordinate and structure factor of $TseP^{C}$ have been deposited in the Protein Data Bank with
396 accession code 8XCL.

397 **Acknowledgements**

This work was supported by funding from National Natural Science Foundation of China (32030001) and National Key R&D Program of China (2020YFA0907200). The funders had no role in study design, data collection and interpretation, or the decision to submit the work for publication.

Author contributions

T.D. conceived the project. Z-H.W., T-T.P., D.Y.W., and X.L. performed research and data analysis. Z--H.W., Y.A., T.Z., and W.Q. performed the crystallography and structural analysis. T.D. and Z-H.W.. wrote the manuscript with assistance from Y.A.

Competing interests

The authors declare no competing interests.

References

1. C. J. L. Murray, *et al*, Global burden of bacterial antimicrobial resistance in 2019: a systematic analysis. *The Lancet* **399**, 629–655 (2022).

2. J. O'Neill, Tackling drug-resistant infections globally: final report and recommendations, *Wellcome Collection* (2016). https://wellcomecollection.org/works/thvwsuba/items.

3. R. A. Bonomo, β-lactamases: a focus on current challenges. *Cold Spring Harb. Perspect. Med.* **7**, a025239 (2017).

4. S. M. Drawz, R. A. Bonomo, Three decades of β-lactamase inhibitors. *Clin. Microbiol. Rev.* **23**, 160–201 (2010).

5. T. M. Brooks, D. Unterweger, V. Bachmann, B. Kostiuk, S. Pukatzki, Lytic activity of the *Vibrio cholerae* type VI secretion toxin VgrG-3 is inhibited by the antitoxin TsaB. *J. Biol. Chem.* **288**, 7618–7625 (2013).

6. T. G. Dong, B. T. Ho, D. R. Yoder-Himes, J. J. Mekalanos, Identification of T6SS-dependent effector and immunity proteins by Tn-seq in *Vibrio cholerae*. *Proc. Natl. Acad. Sci. U. S. A.* **110**, 2623–2628 (2013).

7. A. B. Russell, R. D. Hood, N. K. Bui, M. LeRoux, W. Vollmer, J. D. Mougous, Type VI secretion delivers bacteriolytic effectors to target cells. *Nature* **475**, 343–347 (2011).

8. J. C. Whitney, S. B. Peterson, J. Kim, M. Pazos, A. J. Verster, M. C. Radey, H. D. Kulasekara, M. Q. Ching, N. P. Bullen, D. Bryant, Y. A. Goo, M. G. Surette, E. Borenstein, W. Vollmer, J. D. Mougous, A broadly distributed toxin family mediates contact-dependent antagonism between gram-positive bacteria. *eLife* **6**, e26938 (2017).

419 9. R. D. Hood, P. Singh, F. Hsu, T. Güvener, M. A. Carl, R. R. S. Trinidad, J. M. Silverman, B. B.
420 Ohlson, K. G. Hicks, R. L. Plemel, M. Li, S. Schwarz, W. Y. Wang, A. J. Merz, D. R. Goodlett, J.
421 D. Mougous, A type VI secretion system of *Pseudomonas aeruginosa* targets a toxin to bacteria.
422 *Cell Host Microbe* **7**, 25–37 (2010).

423 10. N.-H. Le, V. Pinedo, J. Lopez, F. Cava, M. F. Feldman, Killing of Gram-negative and Gram-
424 positive bacteria by a bifunctional cell wall-targeting T6SS effector. *Proc. Natl. Acad. Sci. U. S. A.*
425 **118**, e2106555118 (2021).

426 11. A. T. Ma, S. McAuley, S. Pukatzki, J. J. Mekalanos, Translocation of a *Vibrio cholerae* type VI
427 secretion effector requires bacterial endocytosis by host cells. *Cell Host Microbe* **5**, 234–243 (2009).

428 12. J. D. Mougous, M. E. Cuff, S. Raunser, A. Shen, M. Zhou, C. A. Gifford, A. L. Goodman, G.
429 Joachimiak, C. L. Ordoñez, S. Lory, T. Walz, A. Joachimiak, J. J. Mekalanos, A virulence locus of
430 *Pseudomonas aeruginosa* encodes a protein secretion apparatus. *Science* **312**, 1526–1530 (2006).

431 13. T.-T. Pei, Y. Kan, Z.-H. Wang, M.-X. Tang, H. Li, S. Yan, Y. Cui, H.-Y. Zheng, H. Luo, X. Liang,
432 T. Dong, Delivery of an Rhs-family nuclease effector reveals direct penetration of the gram-positive
433 cell envelope by a type VI secretion system in *Acidovorax citrulli*. *mLife* **1**, 66–78 (2022).

434 14. S. Pukatzki, A. T. Ma, D. Sturtevant, B. Krastins, D. Sarracino, W. C. Nelson, J. F. Heidelberg, J.
435 J. Mekalanos, Identification of a conserved bacterial protein secretion system in *Vibrio cholerae*
436 using the *Dictyostelium* host model system. *Proc. Natl. Acad. Sci. U. S. A.* **103**, 1528–1533 (2006).

437 15. K. Trunk, J. Peltier, Y.-C. Liu, B. D. Dill, L. Walker, N. A. R. Gow, M. J. R. Stark, J. Quinn, H.
438 Strahl, M. Trost, S. J. Coulthurst, The type VI secretion system deploys antifungal effectors against
439 microbial competitors. *Nat. Microbiol.* **3**, 920–931 (2018).

440 16. M. Basler, M. Pilhofer, P. G. Henderson, J. G. Jensen, J. Mekalanos, Type VI secretion requires a
441 dynamic contractile phage tail-like structure. *Nature* **483**, 182–186 (2012).

442 17. Y. R. Brunet, A. Zoued, F. Boyer, B. Douzi, E. Cascales, The type VI secretion TssEFGK-VgrG
443 phage-like baseplate is recruited to the TssJLM membrane complex via multiple contacts and serves
444 as assembly platform for tail tube/sheath polymerization. *PLoS Genet.* **11**, e1005545 (2015).

445 18. B. T. Ho, T. G. Dong, J. J. Mekalanos, A view to a kill: the bacterial type 6 secretion system. *Cell*
446 *Host Microbe* **15**, 9–21 (2014).

447 19. J. Wang, M. Brodmann, M. Basler, Assembly and subcellular localization of bacterial type VI
448 secretion systems. *Annu. Rev. Microbiol.* **73**, 621–638 (2019).

449 20. S. Pukatzki, A. T. Ma, D. Sturtevant, B. Krastins, D. Sarracino, W. C. Nelson, J. F. Heidelberg, J.
450 J. Mekalanos, Identification of a conserved bacterial protein secretion system in *Vibrio cholerae*
451 using the *Dictyostelium* host model system. *Proc. Natl. Acad. Sci. U. S. A.* **103**, 1528–1533 (2006).

452 21. M. M. Shneider, S. A. Buth, B. T. Ho, M. Basler, J. J. Mekalanos, P. G. Leiman, PAAR-repeat
453 proteins sharpen and diversify the type VI secretion system spike. *Nature* **500**, 350–353 (2013).

454 22. F. Kamal, X. Liang, K. Manera, T.-T. Pei, H. Kim, L. G. Lam, A. Pun, S. J. Hersch, T. G. Dong,
455 Differential cellular response to translocated toxic effectors and physical penetration by the type VI
456 secretion system. *Cell Rep.* **31**, 107766 (2020).

457 23. X. Liang, F. Kamal, T.-T. Pei, P. Xu, J. J. Mekalanos, T. G. Dong, An onboard checking mechanism
458 ensures effector delivery of the type VI secretion system in *Vibrio cholerae*. *Proc. Natl. Acad. Sci.*
459 *U. S. A.* **116**, 23292–23298 (2019).

460 24. A. Vettiger, M. Basler, Type VI secretion system substrates are transferred and reused among sister
461 cells. *Cell* **167**, 99-110.e12 (2016).

462 25. X. Liang, R. Moore, M. Wilton, M. J. Q. Wong, L. Lam, T. G. Dong, Identification of divergent
463 type VI secretion effectors using a conserved chaperone domain. *Proc. Natl. Acad. Sci. U. S. A.* **112**,
464 9106–9111 (2015).

465 26. S. Pukatzki, A. T. Ma, A. T. Revel, D. Sturtevant, J. J. Mekalanos, Type VI secretion system
466 translocates a phage tail spike-like protein into target cells where it cross-links actin. *Proc. Natl.*
467 *Acad. Sci. U. S. A.* **104**, 15508–15513 (2007).

468 27. A. B. Russell, P. Singh, M. Brittnacher, N. K. Bui, R. D. Hood, M. A. Carl, D. M. Agnello, S.
469 Schwarz, D. R. Goodlett, W. Vollmer, J. D. Mougous, A widespread bacterial type VI secretion
470 effector superfamily identified using a heuristic approach. *Cell Host Microbe* **11**, 538–549 (2012).

471 28. D. Salomon, L. N. Kinch, D. C. Trudgian, X. Guo, J. A. Klimko, N. V. Grishin, H. Mirzaei, K. Orth,
472 Marker for type VI secretion system effectors. *Proc. Natl. Acad. Sci. U. S. A.* **111**, 9271–9276
473 (2014).

474 29. M. Si, C. Zhao, B. Burkinshaw, B. Zhang, D. Wei, Y. Wang, T. G. Dong, X. Shen, Manganese
475 scavenging and oxidative stress response mediated by type VI secretion system in *Burkholderia*
476 *thailandensis*. *Proc. Natl. Acad. Sci. U. S. A.* **114**, E2233–E2242 (2017).

477 30. J. C. Whitney, D. Quentin, S. Sawai, M. LeRoux, B. N. Harding, H. E. Ledvina, B. Q. Tran, H.
478 Robinson, Y. A. Goo, D. R. Goodlett, S. Raunser, J. D. Mougous, An interbacterial $NAD(P)^+$
479 glycohydrolase toxin requires elongation factor Tu for delivery to target cells. *Cell* **163**, 607–619
480 (2015).

481 31. X. Yu, Y. Yan, J. Zeng, Y. Liu, X. Sun, Z. Wang, L. Li, T6SS nuclease effectors in *Pseudomonas*
482 *syringae* act as potent antimicrobials in interbacterial competition. *J. Bacteriol.* **206**, e00273-23
483 (2024).

484 32. S. Das, S. Das, P. P. Rath, A. Banerjee, S. Gourinath, A. K. Mukhopadhyay, S. Maiti, Hemolysin
485 coregulated protein (HCP) from *Vibrio cholerae* interacts with the host cell actin cytoskeleton. *ACS*
486 *Infect. Dis.* **10**, 2886–2898 (2024).

487 33. W. Vollmer, D. Blanot, M. A. De Pedro, Peptidoglycan structure and architecture. *FEMS Microbiol.*
488 *Rev.* **32**, 149–167 (2008).

489 34. J. Ma, M. Sun, Z. Pan, C. Lu, H. Yao, Diverse toxic effectors are harbored by *vgrG* islands for
490 interbacterial antagonism in type VI secretion system. *Biochim. Biophys. Acta BBA - Gen. Subj.*
491 **1862**, 1635–1643 (2018).

492 35. R. E. Hernandez, R. Gallegos-Monterrosa, S. J. Coulthurst, Type VI secretion system effector
493 proteins: Effective weapons for bacterial competitiveness. *Cell. Microbiol.* **22**, e13241 (2020).

494 36. J. C. Whitney, S. Chou, A. B. Russell, J. Biboy, T. E. Gardiner, M. A. Ferrin, M. Brittnacher, W.
495 Vollmer, J. D. Mougous, Identification, structure, and function of a novel type VI secretion
496 septidoglycan glycoside hydrolase effector-immunity pair. *J. Biol. Chem.* **288**, 26616–26624 (2013).

497 37. P.-L. Chen, B. Lamy, W.-C. Ko, *Aeromonas dhakensis*, an increasingly recognized human pathogen.
498 *Front. Microbiol.* **7**, 793 (2016).

499 38. H. Kitagawa, H. Ohge, L. Yu, S. Kayama, T. Hara, S. Kashiyama, T. Kajihara, J. Hisatsune, T.
500 Sueda, M. Sugai, *Aeromonas dhakensis* is not a rare cause of *Aeromonas* bacteremia in Hiroshima,
501 Japan. *J. Infect. Chemother.* **26**, 316–320 (2020).

502 39. X. Liang, H.-Y. Zheng, Y.-J. Zhao, Y.-Q. Zhang, T.-T. Pei, Y. Cui, M.-X. Tang, P. Xu, T. Dong,
503 VgrG spike dictates PAAR requirement for the assembly of the type VI secretion system. *J.*
504 *Bacteriol.*, e0035622 (2023).

505 40. X. Liang, T.-T. Pei, Z.-H. Wang, W. Xiong, L.-L. Wu, P. Xu, S. Lin, T. G. Dong, Characterization
506 of lysozyme-like effector TseP reveals the dependence of type VI secretion system (T6SS) secretion
507 on effectors in *Aeromonas dhakensis* strain SSU. *Appl. Environ. Microbiol.* **87**, e0043521 (2021).

508 41. T.-T. Pei, H. Li, X. Liang, Z.-H. Wang, G. Liu, L.-L. Wu, H. Kim, Z. Xie, M. Yu, S. Lin, P. Xu, T.
509 G. Dong, Intramolecular chaperone-mediated secretion of an Rhs effector toxin by a type VI
510 secretion system. *Nat. Commun.* **11**, 1865 (2020).

511 42. G. Suarez, J. C. Sierra, J. Sha, S. Wang, T. E. Erova, A. A. Fadl, S. M. Foltz, A. J. Horneman, A.
512 K. Chopra, Molecular characterization of a functional type VI secretion system from a clinical
513 isolate of *Aeromonas hydrophila*. *Microb. Pathog.* **44**, 344–361 (2008).

514 43. M. van Kempen, S. S. Kim, C. Tumescheit, M. Mirdita, J. Lee, C. L. M. Gilchrist, J. Söding, M.
515 Steinegger, Fast and accurate protein structure search with Foldseek. *Nat. Biotechnol.* **42**, 243–246
516 (2024).

517 44. K. Maenaka, M. Matsushima, H. Song, F. Sunada, K. Watanabe, I. Kumagai, Dissection of protein-
518 carbohydrate interactions in mutant hen egg-white lysozyme complexes and their hydrolytic activity.
519 *J. Mol. Biol.* **247**, 281–293 (1995).

520 45. E. Altindis, T. Dong, C. Catalano, J. Mekalanos, Secretome analysis of *Vibrio cholerae* type VI
521 secretion system reveals a new effector-immunity pair. *mBio* **6**, e00075 (2015).

522 46. S. J. Hersch, N. Watanabe, M. S. Stietz, K. Manera, F. Kamal, B. Burkinshaw, L. Lam, A. Pun, M.
523 Li, A. Savchenko, T. G. Dong, Envelope stress responses defend against type six secretion system
524 attacks independently of immunity proteins. *Nat. Microbiol.* **5**, 706–714 (2020).

525 47. S. Chou, N. K. Bui, A. B. Russell, K. Lexa, T. E. Gardiner, M. LeRoux, W. Vollmer, J. D. Mougous,
526 Structure of a peptidoglycan amidase effector targeted to Gram-negative bacteria by the type VI
527 secretion system. *Cell Rep.* **1**, 656–664 (2012).

528 48. A. Radkov, A. L. Sapiro, S. Flores, C. Henderson, H. Saunders, R. Kim, S. Massa, S. Thompson,
529 C. Mateusiak, J. Biboy, Z. Zhao, L. M. Starita, W. L. Hatleberg, W. Vollmer, A. B. Russell, J.-P.
530 Simorre, S. Anthony-Cahill, P. Brzovic, B. Hayes, S. Chou, Antibacterial potency of type VI
531 amidase effector toxins is dependent on substrate topology and cellular context. *eLife* **11**, e79796
532 (2022).

533 49. X. Liang, T.-T. Pei, H. Li, H.-Y. Zheng, H. Luo, Y. Cui, M.-X. Tang, Y.-J. Zhao, P. Xu, T. Dong,
534 VgrG-dependent effectors and chaperones modulate the assembly of the type VI secretion system.
535 *PLOS Pathog.* **17**, e1010116 (2021).

536 50. C.-F. Wu, Y.-W. Lien, D. Bondage, J.-S. Lin, M. Pilhofer, Y.-L. Shih, J. H. Chang, E.-M. Lai,
537 Effector loading onto the VgrG carrier activates type VI secretion system assembly. *EMBO Rep.*
538 **21**, e47961 (2019).

539 51. M. S. Stietz, X. Liang, H. Li, X. Zhang, T. G. Dong, TssA–TssM–TagA interaction modulates type
540 VI secretion system sheath-tube assembly in *Vibrio cholerae*. *Nat. Commun.* **11** (2020).

541 52. C. E. Outten, and T. V. O'Halloran, Femtomolar sensitivity of metalloregulatory proteins
542 controlling zinc homeostasis. *Science* **292**, 2488–2492 (2001).

543 53. M.-X. Tang, T.-T. Pei, Q. Xiang, Z.-H. Wang, H. Luo, X.-Y. Wang, Y. Fu, T. Dong, Abiotic factors
544 modulate interspecies competition mediated by the type VI secretion system effectors in *Vibrio*
545 *cholerae*. *ISME J.* **16**, 1765–1775 (2022).

546 54. P. D. Adams, R. W. Grosse-Kunstleve, L.-W. Hung, T. R. Ioerger, A. J. McCoy, N. W. Moriarty,
547 R. J. Read, J. C. Sacchettini, N. K. Sauter, T. C. Terwilliger, PHENIX: building new software for
548 automated crystallographic structure determination. *Acta Crystallogr. D Biol. Crystallogr.* **58**,
549 1948–1954 (2002).

550 55. P. Emsley, K. Cowtan, Coot: model-building tools for molecular graphics. *Acta Crystallogr. D Biol.*
551 *Crystallogr.* **60**, 2126–2132 (2004).

552 56. Schrödinger, LLC, The PyMOL molecular graphics system, version 1.8 (2015).

553 57. B. Glauner, Separation and quantification of muropeptides with high-performance liquid
554 chromatography. *Anal. Biochem.* **172**, 451–464 (1988).

555 58. L. Yang, Y. Gan, L. Yang, B. Jiang, J. Tang, Peptidoglycan hydrolysis mediated by the amidase
556 AmiC and its LytM activator NlpD is critical for cell separation and virulence in the phytopathogen
557 *Xanthomonas campestris*. *Mol. Plant Pathol.* **19**, 1705–1718 (2018).

558 59. Stephen F. Altschul, Warren Gish, Webb Miller, Eugene W. Myers, David J. Lipman, Basic local
559 alignment search tool. *J. Mol. Biol.* **215**, 403–410 (1990).

560 60. Jana Trifinopoulos, Lam-Tung Nguyen, Arndt von Haeseler, Bui Quang Minh, UniProt: the
561 Universal Protein Knowledgebase in 2023. *Nucleic Acids Res.* **51**, D523–D531 (2023).

562 61. J. Trifinopoulos, L.-T. Nguyen, A. von Haeseler, B. Q. Minh, W-IQ-TREE: a fast online
563 phylogenetic tool for maximum likelihood analysis. *Nucleic Acids Res.* **44**, W232–W235 (2016).

564 62. F. Sievers, A. Wilm, D. Dineen, T. J. Gibson, K. Karplus, W. Li, R. Lopez, H. McWilliam, M.
565 Remmert, J. Söding, J. D. Thompson, D. G. Higgins, Fast, scalable generation of high-quality
566 protein multiple sequence alignments using Clustal Omega. *Mol. Syst. Biol.* **7**, 539 (2011).

567 63. X. Robert, P. Gouet, Deciphering key features in protein structures with the new ENDscript server.
568 *Nucleic Acids Res.* **42**, W320–W324 (2014).

Correspondence and request for materials should be addressed to T. Dong.

Figure legends

Figure 1. Structural roles and independent secretion of TseP domains. A, Secretion analysis of TseP, $TseP^N$, and $TseP^C$ in the SSU triple effector deletion mutant (Δ*3eff*). A schematic of the TseP N-terminus ($TseP^N$, 1-603 aa) and C-terminus ($TseP^C$, 604-845 aa) is depicted at the top. Hcp serves as a positive control for T6SS secretion. Hcp, RpoB, and 3V5-tagged TseP proteins were detected using specific antibodies. **B,** Time-lapse imaging of VipA-sfGFP signals in the Δ*3eff* mutant complemented with different TseP variants. Each sample was captured every 10 s for 5 min and temporally color-coded. Color scale used to temporally color code the VipA-sfGFP signals is shown at the bottom. A 30- × 30-μm representative field of cells is shown. Scale bars, 5 μm. **C,** Statistical analysis of T6SS sheath assemblies in the Δ*3eff* mutant complemented with different TseP variants. Error bars indicate the mean ± standard deviation of three biological replicates, and statistical significance was calculated using a two-tailed Student's *t*-test. ns, not significant; **, $P<0.01$. **D,** Secretion analysis of TseP, $TseP^N$, and $TseP^C$ in SSU wild type, Δ*vasK*, Δ*tseP*, and Δ*3eff* mutants. For **B** and **D**, TseP, $TseP^N$, and $TseP^C$ were tagged with a 3V5 C-terminal tag and expressed on pBAD vectors. RpoB serves as an equal loading and autolysis control. **E,** Pull-down analysis of VgrG2 with TseP, $TseP^N$, and $TseP^C$. His-tagged VgrG2 and 3V5-tagged TseP, $TseP^N$, or $TseP^C$ were used. His-tagged sfGFP and 3V5-tagged MBP were used as controls.

Figure 2. Functional analysis of TseP reveals an amidase activity. A, *In vitro* amidase activity of the TseP, $TseP^N$, $TseP^C$, and the lysozyme inactivated mutants $TseP^{E663A}$ and $TseP^{C\text{-}E663A}$. Cell-wall digestion products after incubation with the TseP or its mutants were analyzed by the UPLC/MS. **B,** MS analysis of cell-wall digestion products (NAM-NAC, tetrapeptides, and tripeptides) following treatment with TseP. **C,** Protein sequence alignment of the TseP amidase domain with other amidase homologs (top), and the structural superimposition of the TseP amidase domain and 3SLU (bottom). Cartoon representations of TseP and 3SLU are shown in green and cyan, respectively. The key residues involved in Zn^{2+} binding are shown in a stick model, and the zinc ion is indicated by the green sphere. **D,** *In vitro* amidase activity of $TseP^N$ and its amidase site mutated variants. **E,** *In vitro* amidase activity of TseP under cationic conditions of 2 mM EDTA, Zn^{2+}, Ca^{2+}, or a combination of both cations. TseP represents protein purified without EDTA treatment while $TseP^{EDTA}$ refers to protein purified in presence of EDTA. **F,** PG digestion analysis of $TseP^N$ with or without TsiP. The immunity protein TsiP was incubated with $TseP^N$ on ice for 12 h before being mixed with PG. Products in **D**, **E**, and **F** were analyzed by

UPLC-QTOF MASS. **G,** Pull-down analysis of TsiP with TseP, $TseP^N$, and $TseP^C$. His-tagged TsiP and 3V5-tagged TseP, $TseP^N$, or $TseP^C$ were used. His-tagged sfGFP and 3V5-tagged MBP were used as controls.

Figure 3. Amidase activity of TseP is not essential for T6SS assembly or lysozyme function. A, Secretion analysis of Hcp in the Δ*3eff* mutant complemented with different TseP variants. RpoB serves as an equal loading and autolysis control. Hcp, RpoB, and 3V5-tagged TseP proteins were detected using specific antibodies. **B,** Time-lapse imaging of VipA-sfGFP signals in the Δ*3eff* mutant complemented with TseP or its amidase-inactive mutant $TseP^{H339A}$. Each sample was captured every 10 s for 5 min and temporally color-coded. Color scale used to temporally color code the VipA-sfGFP signals is shown at the right. A 30 × 30 μm representative field of cells is shown. Scale bars, 5 μm. **C,** Competition analysis of the Δ*3eff* mutant complemented with different TseP variants. Competition assays were repeated once. **D,** Glycoside hydrolase activity of the TseP, $TseP^C$ and amidase-inactive mutant $TseP^{H339A}$. The error bars indicate the mean ± standard deviation of three biological replicates.

Figure 4. TseP homologs showed the same *in vitro* PG-hydrolysis activity with the TseP. A, Maximum-likelihood phylogeny of TseP homologs. Phylogeny was constructed using the IQ-tree web server with bootstrap 1000 times. Proteins tested in this study are highlighted in red. **B,** Amidase activity analysis of TseP homologs. **C,** *In vitro* PG-hydrolysis activity of the TseP homologs. Products in **B** and **C** were analyzed through UPLC-QTOF MASS. **D,** GC contents of the *tseP* gene cluster and *AHA_1849* gene cluster. **E,** Summary of $TseP^N$ and $TseP^C$ homologs output by Foldseek Search server. **F,** Structure alignments of TseP and homologs WL1483_2262 and DSB67_24810.

Figure 5. Crystal structure of $TseP^C$. A, Enzymatic activity of TseP, $TseP^C$, and lysozyme in hydrolyzing purified *E. coli* PG. The error bars indicate the mean standard deviation of three biological replicates. **B,** The overall structure of the $TseP^C$. The small lobe and large lobe are shown in cyan and green, respectively, with the connecting loop depicted in red. **C,** Electrostatic potential maps of $TseP^C$ with the Y720, R723, and K796 shown as a stick model. The electrostatic surface potentials are colored red for negative charges, blue for positive charges, and white for neutral residues. **D,** Structural comparison of $TseP^C$ and lysozyme (PDB ID: 1LZC). The catalytic sites are shown as a stick model. **E,** *E. coli* PG digestion analysis of $TseP^C$ and $TseP^{C\text{-}E663D}$ mutant. Error bars indicate the mean ± standard deviation of three biological replicates, and statistical significance was calculated using a two-tailed Student's *t*-test. ****, $P<0.0001$.

Figure 6. Modification of surface charge enables TseP^{C} to kill Gram-positive bacteria. A, *B. subtilis* PG digestion analysis of TseP and TseP^{C}. PG was treated with 0.25 M NaOH for 12 h at 37 °C to remove cross-linked peptides and teichoic acid. The lysis percentage was calculated by detecting the changes of OD_{600} during 1 h. The hen-egg lysozyme was used as a positive control. **B,** Electrostatic potential maps of the TseP^{C} and TseP^{C4+}. The active sites and the mutation region are highlighted in red circles. The negatively charged residues D604, E609, D841, and E845 in the mutation region are shown as a stick model and colored in green, and lysines are colored in cyan. **C,** *In vitro* PG-hydrolysis activity of the TseP^{C} and TseP^{C4+}. RBB-labelled *E. coli* PG was used as the substrate and the lysis percentage was detected by dye release. **D,** *B. subtilis* PG digestion analysis of TseP^{C} and TseP^{C4+}. Exponential phase *B. subtilis* cells (OD_{600}~1.0) were used as substrate. The lysis percentage was calculated by detecting the changes of OD_{600} during 1 h with the enzyme concentration at 100 nM. **E,** Secretion analysis of TseP^{C} and TseP^{C4+} in the Δ*tseP* mutant. RpoB serves as an equal loading and autolysis control. RpoB and 3V5-tagged TseP^{C} proteins were detected using specific antibodies. **F,** Statistical analysis of *B. subtilis* cells in the competition assays. Error bars of statistical analysis in **A**, **C**, **D**, and **F** indicate the mean ± standard deviation of three biological replicates, and statistical significance was calculated using a two-tailed Student's *t*-test. ns, not significant; *, $P<0.05$; **, $P<0.01$; ****, $P<0.0001$.

Figure 7. Model of TseP dual functions and engineering. This schematic illustrates the dual amidase-lysozyme activities of TseP and demonstrates an effective engineering strategy to enhance T6SS and its effector capabilities. The T6SS can independently secrete both the N- and C-terminal domains, with multiple evidence suggesting an evolutionary fusion event. These domains interact directly with the upstream-encoded carrier protein VgrG2 for secretion. TseP^{N}, the N-terminal domain, functions as a Zn^{2+}-dependent amidase, while the C-terminal domain, TseP^{C}, exhibits lysozyme activities. However, in its native form, TseP^{C} does not lyse Gram-positive *B. subtilis* cells. Through structural-guided design, TseP^{C} was engineered to create TseP^{C4+} by altering its surface charge. This modification enables TseP^{C4+} to lyse *B. subtilis* cells without affecting its T6SS-dependent secretion. Consequently, the T6SS-equipped cell acquires the ability to lyse *B. subtilis* in a contact-independent manner. Given the diversity of TseP-like effectors and T6SS species, this approach holds significant potential for modulating interspecies competition and combating antimicrobial resistance.

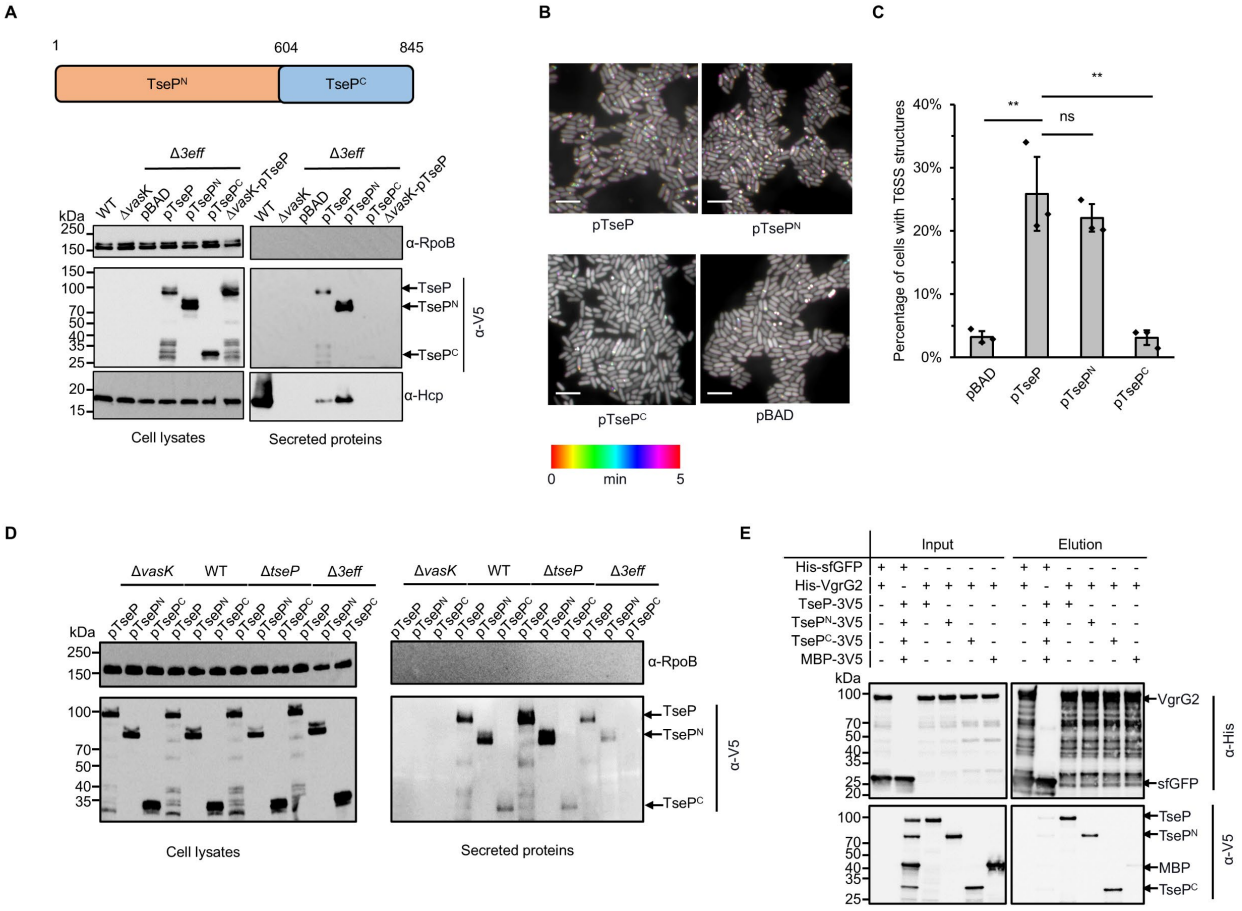
A
1
604
845
TseP^N
TseP^C
Δ3eff
Δ3eff
WT
ΔvasK
pBAD
pTseP
pTseP^N
pTseP^C
ΔvasK-pTseP
kDa
250
150
α-RpoB
100
70
50
40
35
25
TseP
TseP^N
TseP^C
α-V5
20
15
α-Hcp
Cell lysates
Secreted proteins
B
pTseP
pTseP^N
pTseP^C
pBAD
0
min
5
C
Percentage of cells with T6SS structures
40%
30%
20%
10%
0%
**
ns
**
pBAD
pTseP
pTseP^N
pTseP^C
D
ΔvasK
WT
ΔtseP
Δ3eff
pTseP
pTseP^N
pTseP^C
kDa
250
150
α-RpoB
100
70
50
40
35
TseP
TseP^N
TseP^C
α-V5
Cell lysates
Secreted proteins
E
Input
Elution
His-sfGFP
His-VgrG2
TseP-3V5
TseP^N-3V5
TseP^C-3V5
MBP-3V5
kDa
100
70
50
40
35
25
20
VgrG2
sfGFP
α-His
TseP
TseP^N
MBP
TseP^C
α-V5

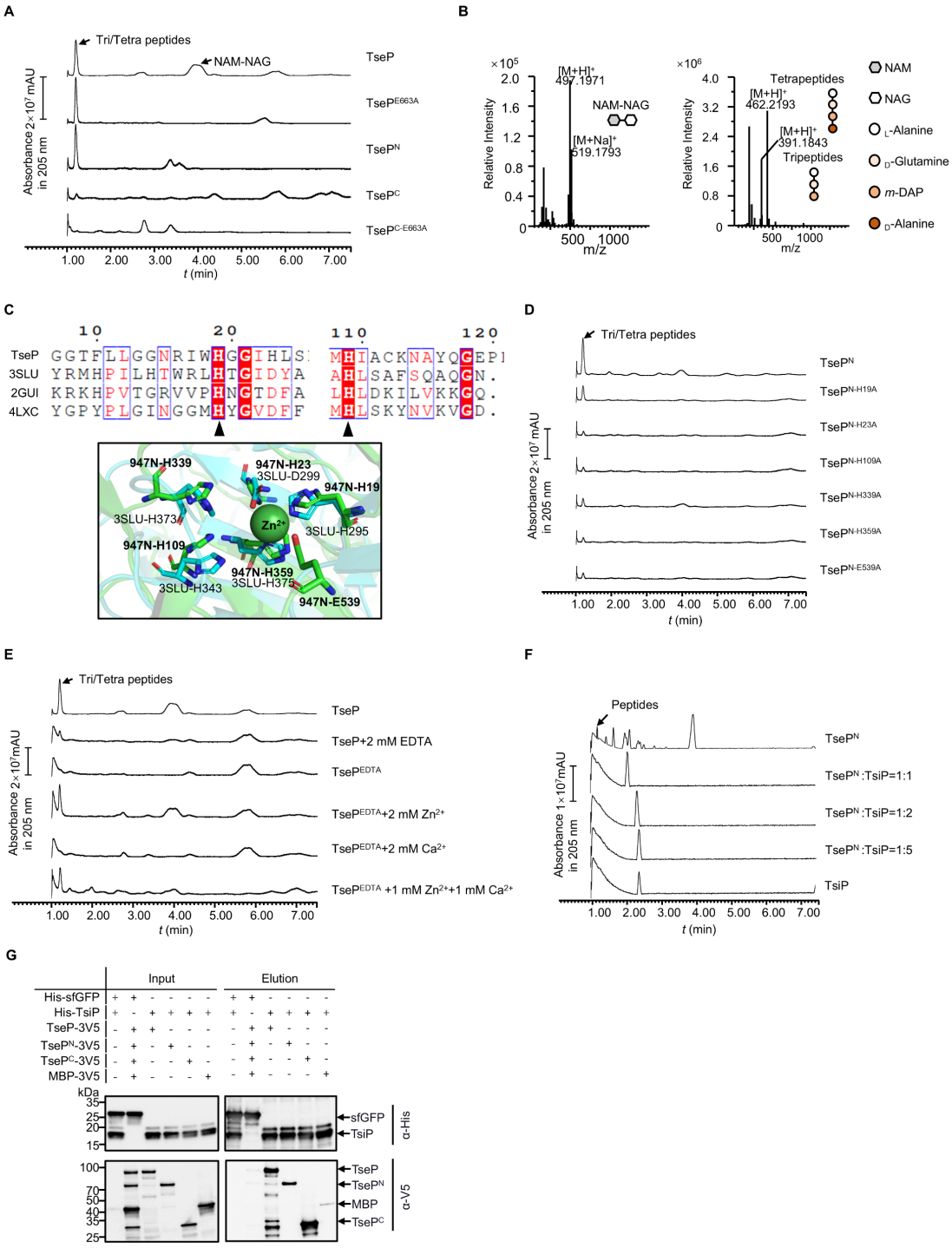
A
Tri/Tetra peptides
NAM-NAG
TseP
TseP^E663A
TseP^N
TseP^C
TseP^C-E663A
Absorbance 2×10^7 mAU in 205 nm
t (min)
B
[M+H]+ 497.1971
NAM-NAG
[M+Na]+ 519.1793
Relative Intensity
m/z
Tetrapeptides
[M+H]+ 462.2193
[M+H]+ 391.1843
Tripeptides
NAM
NAG
L-Alanine
D-Glutamine
m-DAP
D-Alanine
C
TseP
3SLU
2GUI
4LXC
947N-H339
947N-H23
3SLU-D299
947N-H19
3SLU-H373
Zn2+
3SLU-H295
947N-H109
947N-H359
3SLU-H375
3SLU-H343
947N-E539
D
Tri/Tetra peptides
TseP^N
TseP^N-H19A
TseP^N-H23A
TseP^N-H109A
TseP^N-H339A
TseP^N-H359A
TseP^N-E539A
E
Tri/Tetra peptides
TseP
TseP+2 mM EDTA
TseP^EDTA
TseP^EDTA+2 mM Zn2+
TseP^EDTA+2 mM Ca2+
TseP^EDTA +1 mM Zn2+ +1 mM Ca2+
F
Peptides
TseP^N
TseP^N :TsiP=1:1
TseP^N :TsiP=1:2
TseP^N :TsiP=1:5
TsiP
G
Input
Elution
His-sfGFP
His-TsiP
TseP-3V5
TseP^N-3V5
TseP^C-3V5
MBP-3V5
kDa
sfGFP
TsiP
α-His
TseP
TseP^N
MBP
TseP^C
α-V5

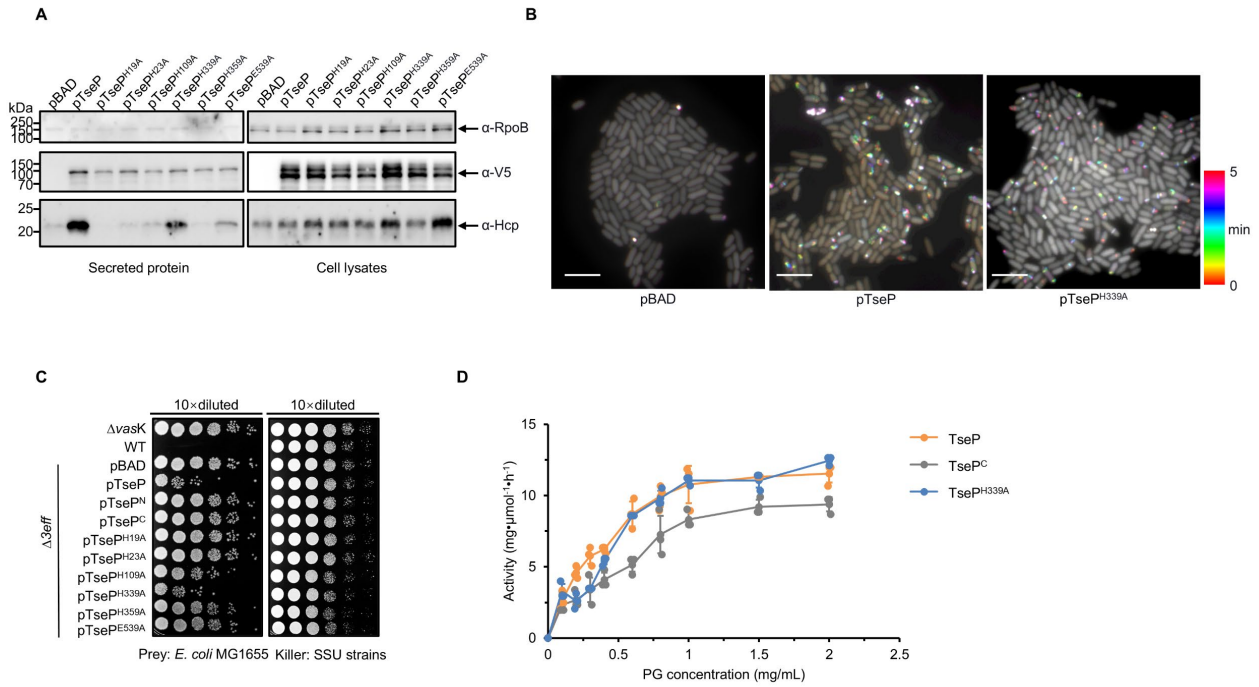
A
kDa
pBAD
pTseP
pTseP^H19A
pTseP^H23A
pTseP^H109A
pTseP^H339A
pTseP^H359A
pTseP^E539A
250
150
100
α-RpoB
150
100
70
α-V5
25
20
α-Hcp
Secreted protein
Cell lysates
B
pBAD
pTseP
pTseP^H339A
5
min
0
C
10×diluted
10×diluted
ΔvasK
WT
pBAD
pTseP
pTseP^N
pTseP^C
pTseP^H19A
pTseP^H23A
pTseP^H109A
pTseP^H339A
pTseP^H359A
pTseP^E539A
Δ3eff
Prey: E. coli MG1655 Killer: SSU strains
D
Activity (mg•μmol⁻¹•h⁻¹)
15
10
5
0
0
0.5
1
1.5
2
2.5
PG concentration (mg/mL)
TseP
TseP^C
TseP^H339A

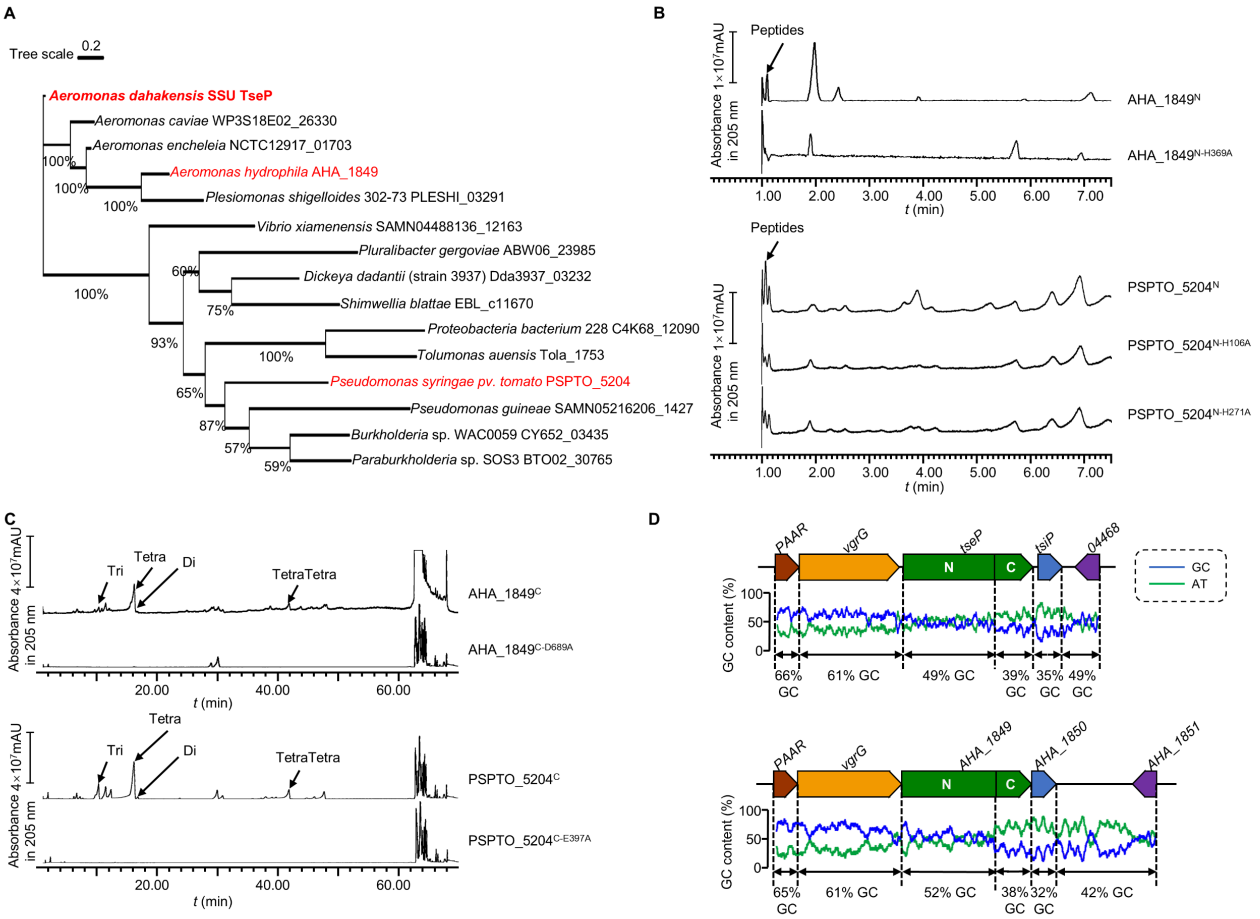

E

Homolog ID	E-Value	RMSD	Coverage (aa position)
Aeromonas schubertii WL1483_2262	4.62e-65	4.23	2-604
Fulvimonas soli C7456_107136	4.20e-24	1.3	606-844
Vibrio campbellii DSB67_24810	1.63e-19	1.88	639-840
Pseudomonas sp. HPB0071 N2J2S6	1.71e-21	1.57	611-844

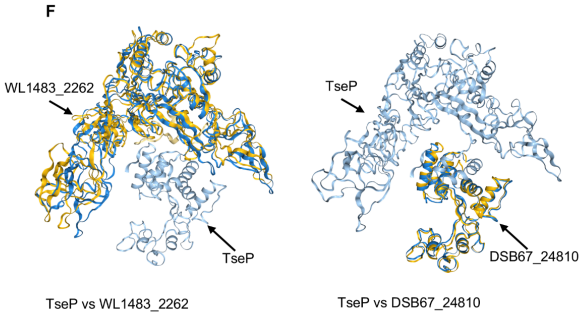

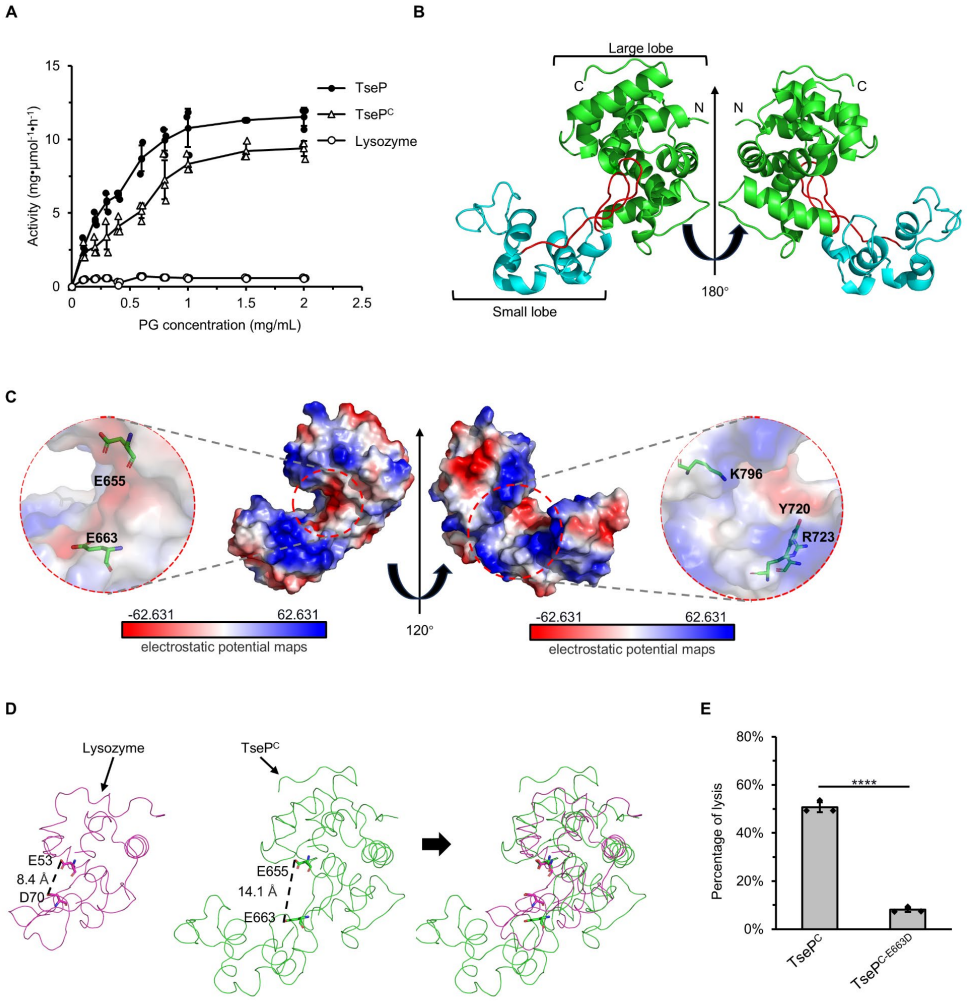
A
Activity (mg•μmol⁻¹•h⁻¹)
PG concentration (mg/mL)
TseP
TseP^C
Lysozyme
B
Large lobe
Small lobe
C
N
180°
C
E655
E663
K796
Y720
R723
-62.631
62.631
electrostatic potential maps
120°
D
Lysozyme
TseP^C
E53
8.4 Å
D70
E655
14.1 Å
E663
E
Percentage of lysis
****
TseP^C
TseP^C-E663D

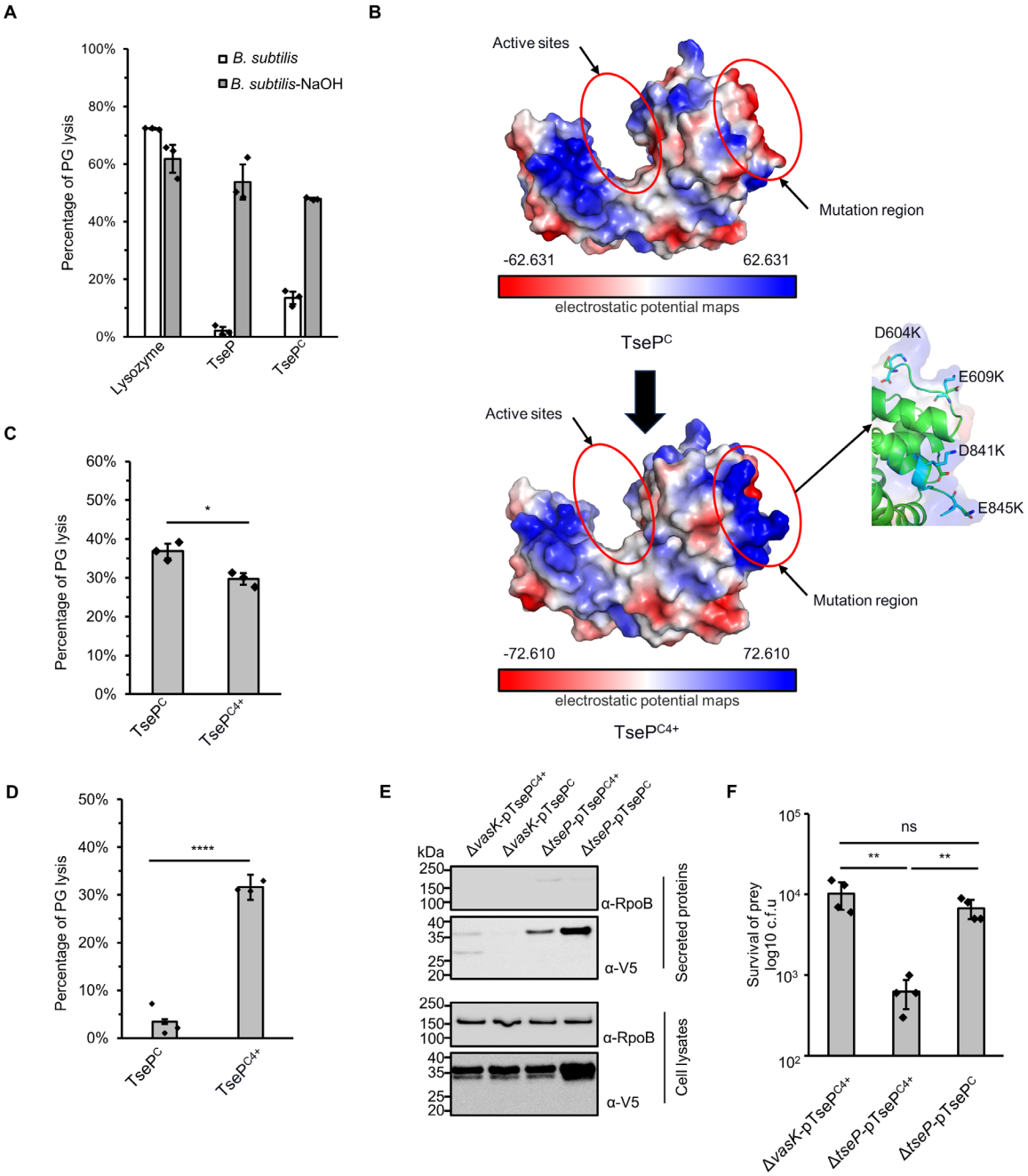
A
100%
80%
60%
40%
20%
0%
Percentage of PG lysis
B. subtilis
B. subtilis-NaOH
Lysozyme
TseP
TsePC
B
Active sites
Mutation region
-62.631
62.631
electrostatic potential maps
TsePC
D604K
E609K
D841K
E845K
Active sites
Mutation region
-72.610
72.610
electrostatic potential maps
TsePC4+
C
60%
50%
40%
30%
20%
10%
0%
Percentage of PG lysis
*
TsePC
TsePC4+
D
50%
40%
30%
20%
10%
0%
Percentage of PG lysis
****
TsePC
TsePC4+
E
kDa
ΔvasK-pTsePC4+
ΔvasK-pTsePC
ΔtseP-pTsePC4+
ΔtseP-pTsePC
250
150
100
α-RpoB
40
35
25
20
α-V5
Secreted proteins
250
150
100
α-RpoB
40
35
25
20
α-V5
Cell lysates
F
10^5
10^4
10^3
10^2
Survival of prey
log10 c.f.u
ns
**
**
ΔvasK-pTsePC4+
ΔtseP-pTsePC4+
ΔtseP-pTsePC

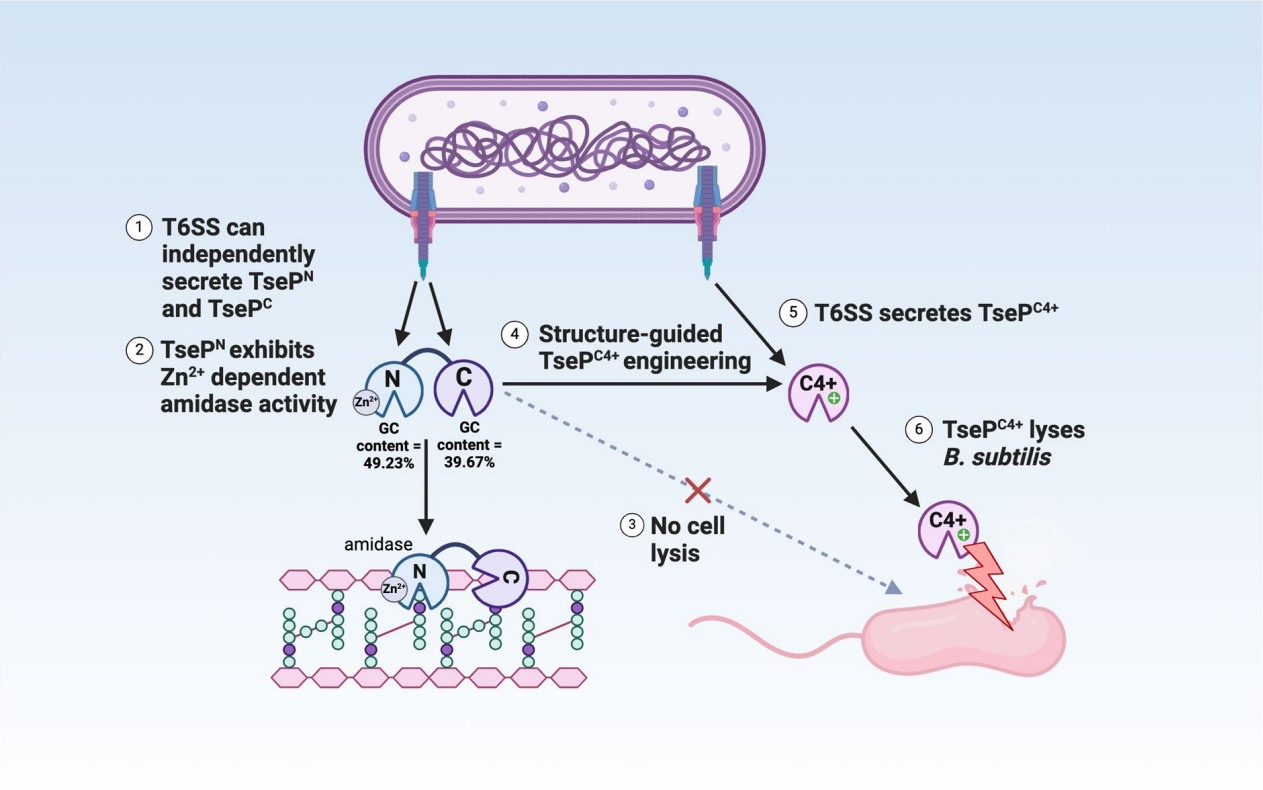
1 T6SS can independently secrete TseP^N and TseP^C
2 TseP^N exhibits Zn2+ dependent amidase activity
N
C
Zn2+
GC content = 49.23%
GC content = 39.67%
amidase
4 Structure-guided TseP^C4+ engineering
5 T6SS secretes TseP^C4+
C4+
6 TseP^C4+ lyses B. subtilis
3 No cell lysis

Table 1. Data collection and refinement statistics of $TseP^C$ crystallization

	$TseP^C$- 8XCL
Data collection	
Space group	*C 2 2 21*
a, b, c(Å)	44.48 138.80 95.83
α, β, γ(°)	90.00 90.00 90.00
Wavelength(Å)	0.97852
Resolution(Å)	47.91 – 2.27(2.40 – 2.27)
$CC_{1/2}$	0.984(0.840)
Unique reflections	25776 (4304)
R_{meas}(%)[a]	23.6(83.6)
Mean $I/\sigma(I)$[a]	6.1(2.6)
Completeness(%)[a]	95.9(99.4)
Multiplicity [a]	12.9(12.0)
Refinement	
Resolution(Å)	47.91 – 2.27
R_{work}/R_{free}[b]	0.189 / 0.227
No.atoms	
Protein	1910
Water	123
Average *B* factors (Å^2)	
Protein	31.72
Water	37.40
R.m.s. deviations	
Bond lengths(Å)	0.007
Bond angles(°)	0.871
Ramachandran plot	
Favored (%)	97.50
Allowed (%)	2.50
Outliers (%)	0.00

[a] The values in parentheses are for the outermost shell.
[b] R_{free} is the R_{work} based on 5% of the data excluded from the refinement.
$R_{meas} = \sum_{hkl}\sqrt{n/(n-1)}\sum_{i=1}^{n}|I_i(hkl) - \langle I(hkl)\rangle| / \sum_{hkl}\sum_i I_i(hkl)$, where $\langle I(hkl)\rangle$ is the mean intensity of a set of equivalent reflections.
$R_{work} = \sum_{hkl}||F_{obs}| - |F_{calc}|| / \sum_{hkl}|F_{obs}|$ where F_{obs} and F_{calc} are observed and calculated structure factors, respectively.